Chemistry Europe
European Chemical Societies Publishing

WILEY VCH

Excellence in Chemistry Research

Announcing our new flagship journal

- Gold Open Access
- Publishing charges waived
- Preprints welcome
- Edited by active scientists

Meet the Editors of *ChemistryEurope*

Luisa De Cola
Università degli Studi di Milano Statale, Italy

Ive Hermans
University of Wisconsin-Madison, USA

Ken Tanaka
Tokyo Institute of Technology, Japan

ChemPhysChem

Research Article
doi.org/10.1002/cphc.202300301

Chemistry Europe
European Chemical Societies Publishing

www.chemphyschem.org

Creating Hydrophobic Foils From Biopolymer Blends Using Mechanical Microimprinting

Hang Liu,*[a] Michaela Zagler,[b] Michael Nase,[b] Katharina Weber,*[a] and Joachim Albrecht*[a]

The surface topography of biodegradable polymer foils is modified by mechanical imprinting on a submillimeter length scale. The created patterns strongly influence the wetting behavior and allow the preparation of hydrophobic surfaces with controlled solid-liquid interaction. A detailed analysis of anisotropic surface patterns reveals that the observed effect arises from a combination of topographical and compositional changes that are introduced to the surface. As a main result it is found that an individual combination of material and structure is required for the production of water-repellent biopolymer foils that are highly attractive for packaging applications.

Introduction

The use of biopolymers has several environmental benefits. Most of them (e.g., lignin[1,2]) are a more sustainable source of raw materials as they are derived from renewable resources such as plants instead of finite petroleum resources used in the production of synthetic polymers. In addition, there are biopolymers like polylactic acid (PLA)[3] that are biodegradable and compostable. These materials do not contribute to the generation of non-biodegradable waste. In general, biopolymers have a wide range of applications in various industries, including packaging, agriculture, and healthcare where sustainability plays an increasing role. In packaging, biodegradable plastic bags and food containers made from biodegradable polymers are becoming increasingly popular as they reduce the environmental impact of plastic waste in the ocean.[4]

Polymer foils are a nearly indispensable element for packaging purposes, in everyday life often met in case of food containers. A main requirement for this application is a reasonably high stability of the material against humidity or water.[5,6,7] This represents a severe drawback for the use of biodegradable polymers, as most of them are hydrophilic and therefore show a low barrier against water vapour permeation. Polymer foils with controlled anisotropic wettability and hydrophobic properties have the advantage of directing fluid flow in a desired direction, improving residual emptying and moisture resistance of packaging.

The surface structuring of polymer films can induce alterations in their wetting behavior. Mechanical imprinting, as a simple and cost-effective method, is employed to achieve surface structuring without the need for chemical treatments. It is ideal for mass production due to its ease of reproducibility. Contact angle (CA) enhancement of various polymer films through mechanical imprinting has been found. In case of an urushi thin film using thermal imprinting of line-line structures a strong anisotropic increase of the CA has been realized.[8] Zhang et al.[9] have shown that an anisotropic structure causes a strong contact angle increase perpendicular to the line direction on the surface of PMMA and PS, and an anisotropic wettability has been found as well. The used structure was generated by thermal imprinting using nanoimprinting lithography (NIL). Xu et al.[10] employed a thermal lamination imprinting method to fabricate a structure on polyethylene films, aiming to produce superhydrophobic polymer surfaces with abrasion resistance and water pressure stability. The mechanical structuring commonly employed in the literature involves first heating the polymer followed by cooling after imprinting. This extended processing time is not efficient for treating packaging materials. Furthermore, there is a scarcity of research regarding the feasibility of mechanical structuring of biopolymer films to improve their wetting properties. In addition, the alteration of surface composition resulting from the mechanical treatment is not considered, making it difficult to conclude whether the change in wetting behavior on the polymer surface is solely attributed to the surface structure or if it is also influenced by the modification of surface composition.

In this work we apply a mechanical imprinting process using micro-engineered stainless-steel stamps to drastically reduce wetting at the surface of biodegradable polymer foils. The goal of method is to change the hydrophilic surface of the polymer into a hydrophobic surface with a large contact angle through mechanical imprinting. Large contact angle or limited contact

[a] H. Liu, Prof. Dr. K. Weber, Prof. Dr. J. Albrecht
Aalen University
Research Institute for Innovative Surfaces FINO
Beethovenstr. 1, 73430 Aalen (Germany)
E-mail: hang.liu@hs-aalen.de
katharina.weber@hs-aalen.de
joachim.albrecht@hs-aalen.de
Homepage: www.hs-aalen.de/FINO/

[b] M. Zagler, Prof. Dr. M. Nase
Hof University of Applied Sciences
Institute for Biopolymers and Sustainability ibp
Alfons-Goppel-Platz 1, 95028 Hof (Germany)

Supporting information for this article is available on the WWW under https://doi.org/10.1002/cphc.202300301

between liquid droplets and solid surfaces leads to reduced adhesion and friction. Such surfaces have ideal liquid-shedding properties and can be used in industries such as glass coatings, microfluidics, and pesticides.[11,12,13] Effective application often relies on both a large contact angle and low contact angle hysteresis, because the contact angle hysteresis (CAH) determines the pinning force of a liquid drop.[13]

Young's equation is a well-known thermodynamic equilibrium condition for a solid-liquid-vapor capillary system: $\gamma_{sl} = \gamma_{sv} + \gamma_{lv}\cos\theta$, where γ_{sv} and γ_{sl} are the solid-vapor and solid-liquid interfacial tensions, γ_{lv} and θ are the liquid surface tension and the contact angle, respectively.[14,15] A key requirement for the equation's derivation is a smooth, homogeneous, and non-deformable solid surface.

In reality, the surface of a solid has a certain roughness and chemical heterogeneity. There are two wetting models to describe the contact angle on such a real surface. The "Wenzel model" accounts for rough surfaces with chemical homogeneity, while the "Cassie-Baxter model" considers the rough surface with chemical heterogeneity.[16,17,18] According to the traditional Wenzel model, the rough surface is completely wetted or filled by the liquid. That means, if the surface is chemically hydrophobic, it will become even more hydrophobic when surface roughness increases the area.[16] The Cassie-Baxter model claims that the wetting liquid does not penetrate into the depressions of the rough surface. The air can remain trapped below the drop and only parts of the entire surface are in contact with the liquid.[17]

The CAH is a crucial characteristic of solid/liquid interfaces, where the established apparent contact angle θ is confined within a specific range, between the advancing (θ_{adv}) and receding contact angles (θ_{rec}). The difference between θ_{adv} and θ_{rec} is referred to as the contact angle hysteresis (θ_{hyst}),[18] which can be attributed to either physical,[18,19,20,21] chemical heterogeneities[18,22,23] in the substrate and the orientation of polar groups at the interface.[24,25]

In this work, wetting at microstructured biopolymer foils will be studied. Microstructuring is performed by an imprinting process using mechanical stamps. To extract the effect of the structuring in all cases line-like structures are generated. An analysis of the wetting behavior with respect to the line direction can identify the role of the structure. Furthermore, the line distance will be varied to determine its effect on the surface wettability and CAH of the biopolymers. Considering both composition and topography of the biopolymer surfaces it will be determined how the line-like structure affects wetting and adhesion behavior.

Material and Methods

Materials

In this study two biopolymers are used, namely a blend of poly(lactic acid) (PLA) – Luminy® LX175 from Total Corbion – and poly(butylene adipate-co-terephthalate) (PBAT) – ecoflex® F Blend C1200 from BASF – in the following called *blend A* and MATER-BI (Mater-Bi® EF51L from Novamont) and kraft lignin, *blend B*. The whole preparation and measurement process is in all cases also performed with a standard polymer, namely low-density polyethylene (LDPE) for better comparison. *Blend A* consists of 60 wt.% PLA and 40 wt.% PBAT. Both polymers have biodegradable properties and PBAT is considered as a flexible polymer for toughening PLA through blending and designed for foil extrusion.[26,27] Furthermore, for *blend B*, MATER-BI and Lignin are melt-blended in a ratio of 70/30. MATER-BI is a biopolymer blend based on PLA and thermoplastic starch (TPS), while Lignin is a natural biopolymer with a complex phenolic macromolecule structure made up of various monomer components.[1,3,28] *Blend A* was prepared by adding the pre-dried polymers PLA and PBAT into two gravimetric feeders of the corotating twin screw extruder LTE 20–44 from Labtech. *Blend B* was also produced on the twin screw extruder from Labtech. The pre-dried MATER-BI and Lignin were compounded in a ratio of 70/30 by means of two gravimetric feeders. The strand pelletizer LZ-120/hp from Labtech, positioned at the end of the water bath, cut the extruded melt strands into pellets. These pellets were afterwards used for the extrusion of the biopolymer foils.

We investigated the wettability of a foil consisting of a PLA/PBAT *blend A* with a ratio of 60/40 and a MATER-BI/Lignin *blend B* with a ratio of 70/30, as with this material composition a continuous blown film extrusion process was possible. Due to the continuous extrusion process an adequate number of foils with similar material properties could be produced, so that it offers good stability for both packaging materials and mechanical structuring applications. Polyethylene (PE) foils are chosen for comparison to ensure the effect of the process.

Methods

Mechanical Structuring Processes

Firstly, line-like microstructures are applied to polymer foils through mechanical imprinting. For that purpose steel (stainless steel 1.4301) stamps are prepared that contain parallel lines with distances of 100 μm to 500 μm. The lines are created using a TRUMP TruMark Station 5000 Laser structuring system. With these stamps PE, PLA/PBAT and MATER-BI/Lignin foils are structured using a tensile testing machine (Typ Z100, Zwick). The process runs at $T = 25\,^{\circ}C$, a force of 50 kN is used for imprinting.

Characterization

Surface Topography

The surface of the polymer foils before the imprinting process is analyzed by Scanning electron microscope (SEM) LEO Gemini 1525 from Zeiss and optical microscopy Polyvar from Reichert-Jung. White-light interferometry (WLI) using a ZYGO ZeGage is conducted to reveal the surface topography of polymer foils and stamp with spatial resolution of a few nanometers along the surface normal.

Differential Scanning Calorimetry (DSC)

The glass transition temperature of the polymer foils is determined using DSC 214 Polyma from NETZSCH-Gerätebau.

Static Contact Angle and Hysteresis Measurements

Static contact-angle measurements and contact angle hystereses are carried out to characterize the wetting behavior of the surface.

The measurements are performed using a DSA100 Krüss CA measurement system. The "Sessile Drop Method" has been used to determine the static contact angle. A deionized water droplet with a volume of 2 μL is deposited on the polymer surface and the water contact angle (WCA) is determined. The contact angle hysteresis is performed according to the Needle-embedded "Sessile Drop Method". For these measurements, the advancing contact angle θadv is measured by adding constant volumes (2 μL) of water to the surface, the receding contact angle θrec is measured by reducing the water volume through the needle with identical volume steps. All experiments are carried out at a temperature of 21 °C and a relative humidity of 38 %. Before each measurement the samples are cleaned with isopropanol. The preparation of anisotropic, line-like structures in combination with angle-dependent drop shape analysis allows the direct access of the microstructure-induced modifications of wetting.

Attenuated Total Reflection Fourier-transform Infrared Spectroscopy (ATR-FTIR) Analysis

Detailed changes in chemical composition of the polymer surface originated by the mechanical imprinting process are analyzed using a ATR-FTIR ALPHA II from BRUKER.

Results and Discussion

Detailed information about the composition of the used polymer blends PLA/PBAT and MATER-BI/Lignin is provided in Figure 1. In the top row an illustration of the phase distribution of the blends is shown, the used colors blue and red will be used for these materials throughout the present work.

Below the schematic illustrations polarization optical microscopy images (second row) and scanning electron microscopy images (third row) are provided of the pristine foils of PLA/PBAT (left) and MATER-BI/Lignin (right). In the optical image of the PLA/PBAT surface the distribution of both constituents can hardly be observed, the image is dominated by anisotropic surface structures that arise from the production process of the foil. While the blown foil extrusion process, polymer chains are orientated and stretched in the machine direction. In case of the MATER-BI/Lignin surface a multi-phase blend system can be identified, islands with typical sizes of about 10 μm are surrounded by a matrix. In this case, the lignin particles disperse in the MATER-BI matrix. The matrix is formed by the partially compatible blend of PLA and TPS (MATER-BI). This means that the matrix is heterogeneous and domains evolve. More detailed information can be extracted from the SEM images below. Here, also the microstructure of the PLA/PBAT blend can be resolved and individual islands with a size of about 1 μm in a homogeneous matrix can be identified. It is noticeable that the spherical droplets of one phase (PBAT) are immersed in the matrix of the other phase (PLA), which exhibits two-phase characteristics. The SEM image of MATER-BI/Lignin in Figure 1 (F) magnifies a single island. Besides the size of about 10 μm it is seen that the islands are elevated from the matrix around. This means that the presence of the different phase leads to a substantially modified surface topography. The fact that the blends consist of separated phases is supported by the

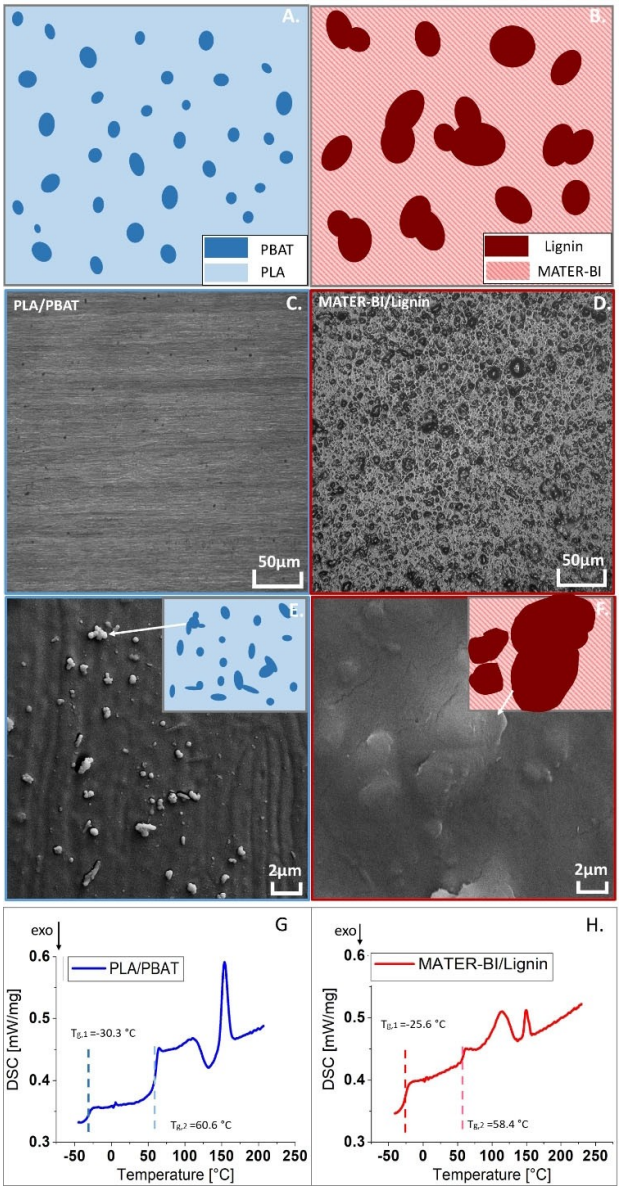

Figure 1. Top row: Illustration of the phase distribution in the biodegradable polymer blends used in this work: PLA/PBAT (left, blue) and MATER-BI/Lignin (right, red). Second row: Optical microscopy in polarized light. Third row: High magnification obtained by scanning electron microscopy. Bottom row: Second heating curves of PLA/PBAT (blue) and MATER-BI/Lignin (red) measured by DSC (see text). The higher glass transition temperature ($T_{g,2}$) refers to the matrix constituent PLA of both blends.

differential scanning calorimetry (DSC) thermograms.[29,30] A single glass transition temperature (T_g) defines a blend containing completely miscible components. Phase-separation in domains manifests itself in separate T_g values, one for each independent component. The Tg measured by DSC are shown in Figure 1 (G) and (H). In each case, two distinctly different glass transitions are observed. The PLA/PBAT blend shows $T_{g,1}$ at −30.3 °C (PBAT) and $T_{g,2}$ at 60.6 °C (PLA).[26] For MATER-BI/Lignin $T_{g,1}$ at −25.6 °C (TPS) and $T_{g,2}$ at 58.4 °C (PLA)[31] are found. A glass transition of Lignin is not visible in the DSC thermogram. This proves that both PLA/PBAT and MATER-BI/Lignin

biopolymer blends are physically only partially miscible. The formation of the blends does not include a chemically interpenetrating network of the components.

Having considered the materials properties Figure 2 displays the surface topography of the used foils. The measurements are performed with a vertical resolution of a few nanometers using white-light interferometry. The surfaces are displayed in false colors in Figure 2. Bright colors refer to elevated areas.

The WLI images show a completely different surface topography for each polymer foil. The PE foil (top) is basically flat with a low density of irregularities of different shape. The surface roughness $R_q = 0.056\ \mu m$ is rather small. PLA/PBAT (center) shows a strong uniaxial surface structure with vertically oriented, individual line-like elements having a typical width of the order of 10 µm. The corresponding roughness $R_q = 0.455\ \mu m$ is large. The MATER-BI/Lignin surface displayed in the bottom panel is characterized by a high density of dot-like elevations. These refer to the islands of lignin that are already described in Figure 1 (F). They lead to a roughness value of $R_q = 0.083\ \mu m$ that is much smaller than for the PLA/PBAT foil.

A micromechanical imprinting technique is used to introduce microstructures into the surface of the foils. Figure 3 illustrates the process.

Figure 3 (A) provides a sketch of the used imprinting technique. Metallic stamps with uniaxial line structures prepared by a Laser structuring process are pressed with high force and without thermal heating onto the surface of the foil. The exact sequence of stamps and materials is illustrated in Figure 3 (A).

A surface of a typical stamp and an example of an imprinted foil are shown in Figures 3 (B) and 3 (C). The images are obtained by white-light interferometry. The false color representation maps show the height distribution of the surface on an area of 843 µm x 843 µm. The bright parts of the image refer to elevated parts of the surface, while dark parts of the image show the deeper parts of the surface. In the stamp surface of Figure 3 (B) there are parallel lines with an individual width of about 50 µm and a depth of nearly 20 µm. The line distance is 400 µm. The topography of the imprinted PLA/PBAT foil (Figure 3 (C)) corresponds as negative to the surface of the stamp. Both surfaces exhibit line-like structures with a distance of 400 µm. In addition, a corresponding horizontal profile is depicted below. The displayed topographies clearly show that

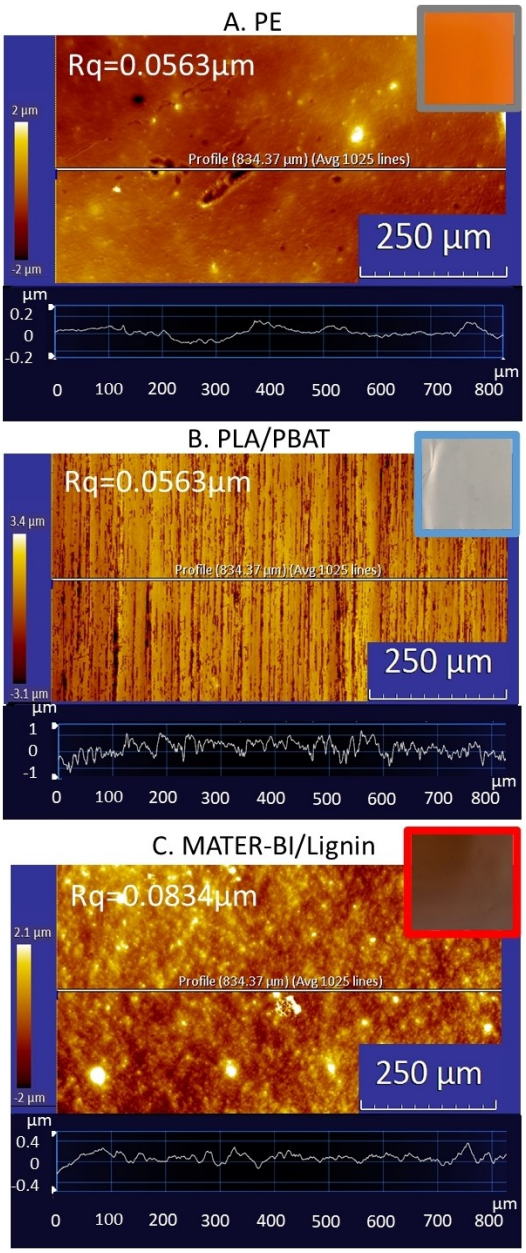

Figure 2. Surface topography of the used foils of PE (A), PLA/PBAT (B) and MATER-BI/Lignin (C). The images are obtained by white-light interferometry, bright colors refer to elevated areas. The profile below is extracted along the solid horizontal line. In the top left corner the quadratic roughness is given, the inset in the top right corner shows a photo of the foil.

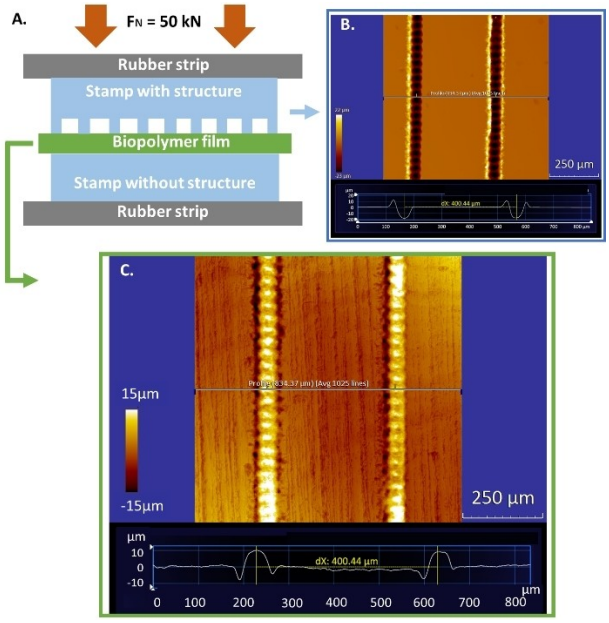

Figure 3. (A) Schematic of the mechanical imprinting process. (B) and (C) WLI images of surface of the stamp and of a created PLA/PBAT surface with groove width 400 µm.

the template is simply embossed into the polymer surface creating a negative image of the template. The comparison reveals that the mechanical process basically reproduces the topography of the stamp.

In Figure 4 the topography of the foils after the imprinting process is studied. The figure depicts a surface profile extracted perpendicular to the line-like structures for all three foils, respectively.

The profiles refer to PLA/PBAT (blue) and MATER-BI/Lignin (red). For comparison the surface profile of the PE foil is depicted in grey. The surface topography is qualitatively similar in all cases. Ordered line-like structures are found at the polymer surface. However, it is revealed that the evolving surface structures exhibit different height scales. The height scale found for PLA/PBAT ranges from −8 μm to 10 μm, for MATER-BI/Lignin from −3 μm to 7 μm and in case of PE from −3 μm to 2 μm. This is of course related to different mechanical properties of the polymers, in particular to different transitions from elastic to plastic deformation. However, there will be no in-depth discussion at this point, the important result is a permanent sculpturing of the surface of the foil. Considering the area in between the imprinted lines we find very smooth surfaces for MATER-BI/Lignin and PE, in case of PLA/PBAT the surface is rather rough. This correlates with the initial roughness of these foils before the imprinting process. The result shows that the roughness of the unstructured sample is largely retained during the mechanical embossing process. Thus, the predominant roughness is not only due to the anisotropic structure, but also to the roughness caused by the manufacturing process.

In the next step it is analyzed how the introduced surface topography affects the wetting process in case of water. For that purpose contact angle measurements are performed using a drop shape analyzer. The used water droplet has a volume of 2 μL and is positioned carefully on a dry surface. The appearing water contact angles (WCA) are analyzed by an image processing software.

Figure 5 illustrates the behavior of a water droplet on a MATER-BI/Lignin surface.

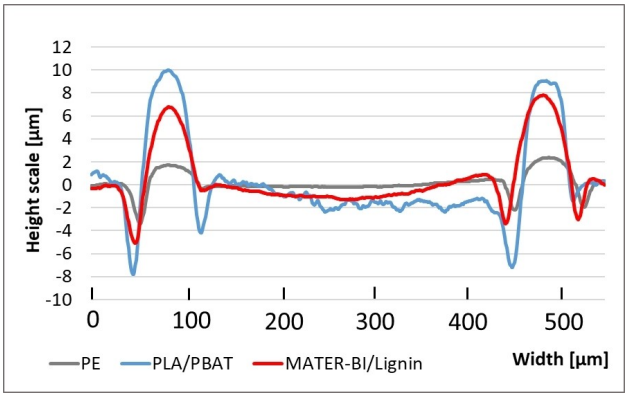

Figure 4. Height profiles of the surface of imprinted PE (grey), PLA/PBAT (blue) and MATER-BI/Lignin (red). A stamp with a line distance of 400 μm has been used. Identical stamps lead to different surface structures.

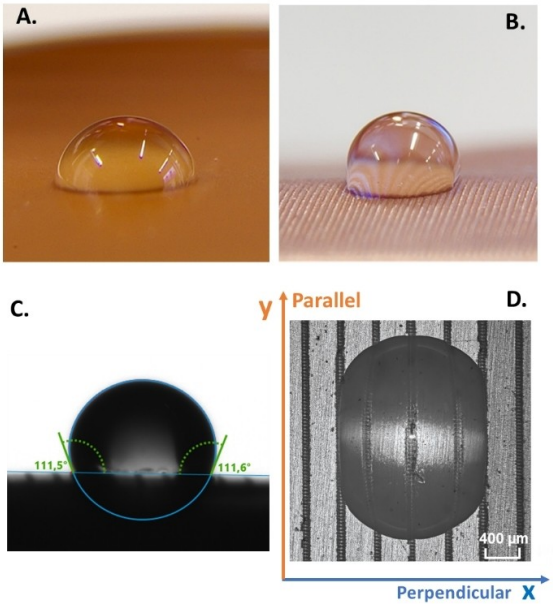

Figure 5. Photographs of water droplets (2 μL) on an unstructured (A) and imprinted (B) MATER-BI/Lignin foil. The microstructure has a line distance of 100 μm. Drop shape with data analysis (side view) from perpendicular direction to the pattern (C). Top view image (PLA/PBAT) of a droplet (2 μL) on the surface with a groove width of 400 μm. The pinning of the drop surface at the lines is clearly visible (D).

The photographs in the top row of Figure 5 show two water droplets with a volume of 2 μL, respectively, placed on a pristine MATER-BI/Lignin surface (left) and on the same foil after the imprinting of a line structure with a line distance of 100 μm. Obviously, the modified surface topography reduces wetting and leads to a significant increase of the WCA values. Figure 5 (C) depicts an individual drop as imaged in the drop shape analyzer. An image processing software calculates the contact angles on both sides of the drop, in the depicted case 111.5° and 111.6°. Further steps of evaluation always use the average of both values. The measurement of the WCAs of each of the materials is always performed in two directions. We define x-direction as the direction perpendicular to the lines and y-direction as the direction parallel to the lines, as illustrated in Figure 5 (D). The top view illustrates the strongly anisotropic wetting behavior on mechanically treated polymer surfaces and the strong interaction between drop surface and line structure. In particular, this means that the contact angle in the direction parallel to the lines is hardly affected by surface imprinting. A significant increase of the contact angles arises in perpendicular direction for all polymer surfaces after mechanical imprinting. This proves that the introduced structures are the main origin of the effect. To correlate surface pattern and wetting the contact angles perpendicular to the line direction are always considered in the following.

The measured contact angles are plotted over the line distance of the imprinted structures for all polymer foils in Figure 6.

The diagram shows the WCA θ for PLA/PBAT (blue), MATER-BI/Lignin (red) and PE (grey) depending on the line distance in

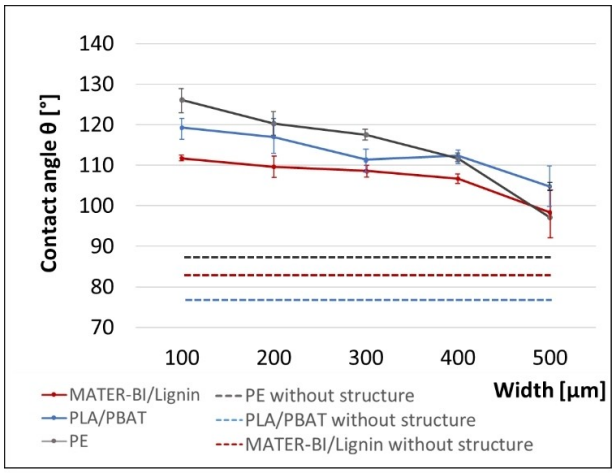

Figure 6. WCA on imprinted surfaces for all polymer foils dependent on the line distance on the surface. The horizontal dashed lines refer to the unstructured foils: WCA by PE = 87.6° ± 0.6°; WCA by PLA/PBAT = 78.5° ± 2.1°; WCA by MATER-BI/Lignin = 82.9° ± 1.2°.

the direction perpendicular to the lines. For comparison, the horizontal dashed lines in corresponding color refer to the pristine surfaces. The x-axis shows the line distance from 100 µm to 500 µm. The y-axis shows the water contact angle (WCA) θ in degrees. All the unstructured materials have hydrophilic surface properties since the water contact angle is below 90°. The introduction of the surface line structures made the polymer foils more hydrophobic in all cases. The original hydrophilic surfaces are transformed into hydrophobic surfaces with apparent contact angles between 110° and 125° in case of the 100 µm structures. For increasing line distances the beneficial effect decreases for all considered polymer foils which is not surprising since the density of the structures decreases. For PE the WCAs decrease from 124.5° to 97.8° from 100 µm to 500 µm line width, in case of PLA/PBAT from 119.4° to 104.7° and for MATER-BI/Lignin from 111.6° to 98.4°. After imprinting is the measured WCA θ for PE largest in the range from 100 µm to 400 µm compared to PLA/PBAT and MATER-BI/Lignin. PLA/PBAT has the largest WCA at 500 µm. MATER-BI/Lignin shows the lowest value. However, the relative change Δθ in the WAC for PLA/PBAT is largest. Here, a relative increase of 56% can be achieved for a line width of 100 µm.

The observed behavior is related to the change of the surface topography due to mechanical imprinting. The prepared line-like structures exhibit inclined flanks with typical slopes between about 30° and 50°. If the equilibrium contact angle (ECA) given by Young's equation forms on an inclined surface the apparent contact angle (ACA) that is seen e.g. in Figure 5a–c can be the sum of ECA and the inclination angle. This explains the increase of the observed CA's. In addition, a decrease of the line density would then lead to a reduction of the effect, as seen in the curves with negative slope in Figure 6.

Further information about the interaction of liquid and surface is collected by hysteresis measurements of the apparent contact angles perpendicular to the line direction. The protocol of the hysteresis measurements is illustrated in Figure 7.

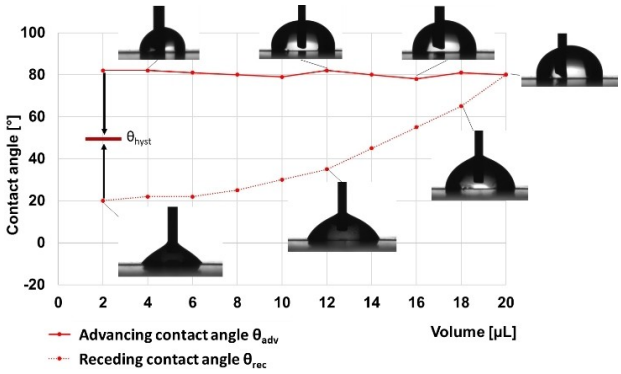

Figure 7. Advancing and receding contact angle measurement for water droplets and corresponding sessile drop images of water droplets on an unstructured MATER-BI/Lignin surface.

A drop with an initial volume of 2 µL is put onto the surface under continuous contact to the water needle. Then in further step, additional 2 µL of water are added. After every step the so called advancing contact angle is measured. This provides the upper red line in the diagram. Having reached 20 µL the needle is used to remove water in steps of 2 µL from the droplet. The interaction of droplet and surface leads to pinning of the drop surface. When removing water a smaller contact angle evolves (bottom red line in the diagram). Finally, the receding curve ends in a horizontal curve that defines the receding contact angle. The difference between advancing and receding contact angle is the contact angle hysteresis θ_{hyst} that is a measure for the interaction of droplet and surface.

The contact angle hysteresis θ_{hyst} is measured for all polymer foils for structural line distances from 100 µm to 500 µm and displayed in Figure 8.

Grey symbols refer to PE, PLA/PBAT is plotted in blue and MATER-BI/Lignin in red. The horizontal dashed lines refer to the pristine surfaces of the polymer foils. It is found that θ_{hyst} most

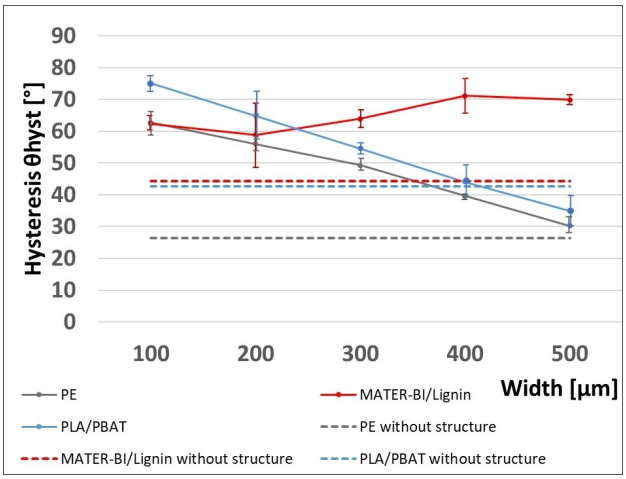

Figure 8. Hysteresis θ_{hys} on imprinted PE, PLA/PBAT and MATER-BI/Lignin surfaces with the line distance from 100 µm to 500 µm and on their unstructured surfaces. The horizontal dashed lines refer to the unstructured foils: θ_{hyst} by PE = 24.9° ± 1.1°; θ_{hyst} by PLA/PBAT = 44.8° ± 1.6°; θ_{hyst} by MATER-BI/Lignin = 46.1° ± 1.8°.

cases the structuring process leads to a substantial increase of θ_{hyst} For PE a hysteresis angle of 30° is found for the 500 µm structures, for the 100 µm structures it is even 63° which is significant more that found for the pristine surface with $\theta_{hyst} =$ 26°. This result is reasonable because the introduced structures lead to additional pinning of the drop surface at the lines and the size of the effect decreases with increasing line distance. Different results are obtained for the biopolymers. The structured PLA/PBAT surface exhibits a similar shape of the θ_{hyst}-curve over the line distance. The PE-curve and the PLA/PBAT curve nearly run parallel. However, for large line distances the hysteresis angles of the structured surfaces are significantly smaller than θ_{hyst} of the pristine foil. The 500 µm surface exhibits a hysteresis angle of 35° which is below the value of 42° for the pristine surface. This means the structuring process reduced the drop-surface interaction and favors the motion of the drop. The MATER-BI/Lignin surface shows a completely different behavior. Here, a nearly constant increase of the hysteresis angle θ_{hyst} of about $30 \pm 5°$ is found independent of the chosen line distance in the imprinting process.

Hysteresis measurements showed that the interaction between the water and the polymer surface strongly increases after mechanical imprinting. This means that the water is partially or completely incorporated into the structure. The latter scenario is described by the Wenzel wetting model of microstructured surfaces. Surfaces exhibiting wetting after the Wenzel model exhibit a high hysteresis in the contact angle.[32,33] There are mainly two reasons for the increase of interaction, first, the structuring process increases the contact area and, second, the modulation of surface elevation leads to pinning of the surface of the droplet.

Different curves for different materials strongly suggest that topographical modifications cannot be the only origin of the observed increase of liquid/surface interaction. There has to be a contribution of the ECA as well. Since the ECA is given according to Young's equation by the interface energy/interface tension between the different contributing phases it is expected that the imprinting process also modified the surface energy of the polymer. In particular, the polar part of the surface energy could be affected since mechanical pressure might lead to a redistribution of chemical bonds near the surface.

ATR-FTIR Analysis

In the following, FTIR spectroscopy is performed to identify compositional changes in the surface of the polymer foils that lead to variations in the polar part of the surface energy. Here, a micropatterned surface with a line distance of $d = 300$ µm was chosen. The FTIR spectra of PE foil before and after imprinting correspond to the typical PE molecular structure and will not be discussed hereafter.

According to the spectra of PLA/PBAT and MATER-BI/Lignin, the same bands are observed before and after mechanical imprinting, with variations in the relative intensity of some bands. Therefore, spectral subtraction is used to examine changes in the intensity of PLA/PBAT (Figure 9 (B)) and MATER-BI/Lignin (Figure 10 (B)) characteristic bands.

The results of FTIR analysis on PLA/PBAT and MATER-BI/Lignin are depicted in Figure 9 (A) and Figure 10 (A). The detailed assignment of peaks to functional groups is presented in the Supporting Information. The FTIR spectrum shows that PLA/PBAT contains two polar groups: carbonyl groups (C═O) and ether functional groups (C–O–C). The FTIR spectrum of MATER-BI/Lignin shows that MATER-BI/Lignin contains hydroxyl (–OH), carbonyl and ether groups. The polarity of these func-

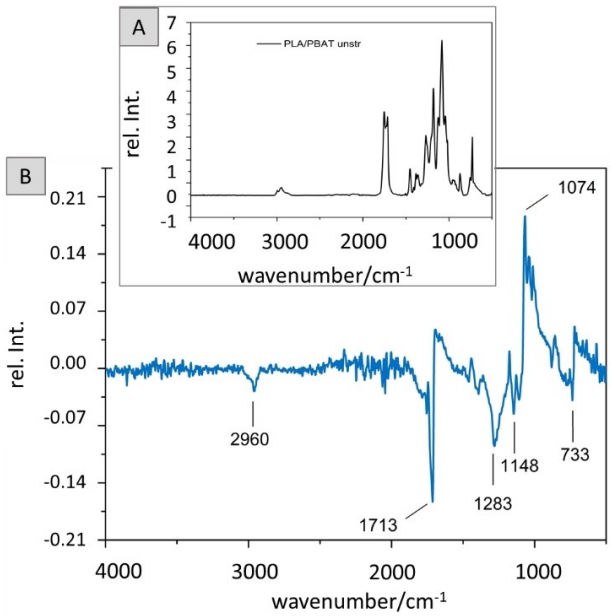

Figure 9. (A) FTIR spectrum of PLA/PBAT. (B) The result of subtracting the spectrum of the unstructured PLA/PBAT from the spectrum of the structured PLA/PBAT.

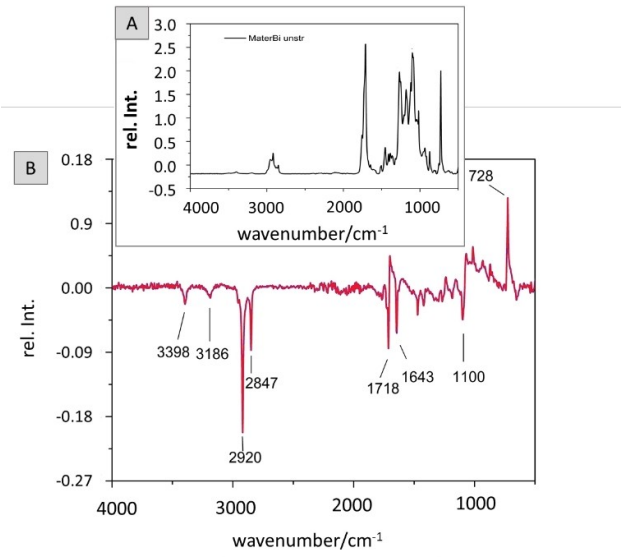

Figure 10. (A) FTIR spectrum of MATER-BI/Lignin. (B) The result of subtracting the spectrum of the unstructured MATER-BI/Lignin from the spectrum of the structured MATER-BI/Lignin.

tional groups is ranked as follows: hydroxyl > carbonyl > ether group. The gradation of the polarity contributions refers to the ability of these groups to undergo hydrogen bonding and dipole-dipole interactions.

The assignments for the FTIR absorption bands for PLA and PBAT with varied intensity upon structuring are presented in Table 1. The corresponding functional groups are divided in polar and dispersive in reference to their influence on the surface polarity of the polymer film. The intensity of dispersive contributions of both PLA and PBAT is attenuated after imprinting. The changes in the intensity of ether-assigned bands reflect an opposite effect on the polarity of the surface, as both decreases and increases are observed. Most strikingly, the intensity of the peak at 1713 cm^{-1} assigned to polar carbonyl groups of PBAT decreases on the imprinted surface. As stated earlier, carbonyl groups have a higher impact on surface polarity than ether groups. This shows that PBAT in the biopolymer blend contributes more to the reduction of polarity on the surface through imprinting compared to PLA.[28]

The assignments for the absorption bands for MATER-BI/Lignin with varied intensity after imprinting are presented in Table 2. Surface structuring leads to both a decrease and an increase in the intensity of the peaks assigned to functional groups with dispersive contribution. More significantly, the intensity of the peaks attributed to the hydroxyl, ester and ether groups decreases upon imprinting. Compared with the unstructured sample, the polarity of the structured surface has decreased overall. It is noteworthy that the two significant peaks at 3186 cm^{-1} and 1718 cm^{-1} belong to lignin. Accordingly, it can be concluded that mechanical imprinting has a significant effect on the distribution of lignin in the polymer (surface vs. bulk) and thus on the polarity of the surface.

These results show that modifications introduced by the presented microimprinting process significantly modify the water-surface interaction. The observed changes in wetting and pinning can not only be understood in terms of a modified surface topography. Moreover, the proposed mechanical surface treatment also directly affect the surface chemistry as seen in FTIR measurements. In case of polymer blends, as considered in this work, the mechanical pressure can lead to a redistribution of individual constituents of the blend in a surface-near region. This directly affects the polarity of the polymer surfaces and, thus, the polar contribution to the surface energy. In case of the micropatterned surfaces that are presented in this work this provides, besides the role of the topography, an additional effect on the liquid-surface interaction of the considered biopolymer foils.

Table 1. Positions and assignments of distinctive FTIR bands related to PLA and PBAT.

	Bands[cm^{-1}]	Functional groups	After imprinting	Assignments
Polar	1713	Carbonyl group	↓	PBAT
	1283/1148/1074	Ether group	↔	PLA und PBAT
Dispersive	2960	C–H	↓	PLA und PBAT
	733	Benzolring	↓	PBAT

Table 2. Positions and assignments of distinctive FTIR bands related to MATER-BI and Lignin.

	Bands[cm^{-1}]	Functional groups	After imprinting	Assignments
Polar	3398	Hydroxyl group	↓	MATER-BI und Lignin
	3186	Hydroxyl group	↓	Lignin
	1718	Carbonyl group	↓	Lignin
	1100	Ether group	↓	MATER-BI
Dispersive	2920/2847	C–H	↓	MATER-BI und Lignin
	1643/728	Benzolring	↑	Lignin

Conclusions

In this work we have shown that mechanical imprinting is an excellent tool to control wetting on biopolymer foils. An appropriate surface pattern allows the increase of the initial contact angle against water by up to a factor of two. Hysteresis measurements revealed that the observed effect is originated both by inhibition of drop growth due to topographical obstacles and by modification of surface composition of the polymer.

From SEM images and DSC results it is evident that both PLA/PBAT and MATER-BI/Lignin blends exhibit only partial physical miscibility. Both blends consist of separated phases. This is consistent with domain formation by the imprinting observed by FTIR spectroscopy. During this process, the surface of the domains changes.

In this study, we consider not only the changes in structure but also the alterations in chemical composition on the surface of the examined biopolymers. This means that our focus is on both the physical and chemical properties of biopolymers. This, in turn, implies that the wetting behavior on the biopolymer surface can be attributed to both its structure and chemical composition.

The preparation of biopolymer foils with improved surface properties offers a promising pathway for the substitution of classical polymer foils in packaging by environment-friendly biopolymers. As a result, the presence of residual product content in the packaging can be reduced, which has a positive impact on its recyclability.

Acknowledgements

The authors are grateful to all members of the Research Institute for Innovative Surfaces FINO for their endless support. Open Access funding enabled and organized by Projekt DEAL.

Conflict of Interests

The authors declare no conflict of interest.

Data Availability Statement

The data that support the findings of this study are available from the corresponding author upon reasonable request.

Keywords: hydrophobic · biopolymer · microimprinting · anisotropic wettability · tribology

[1] C. Carmona, P. Langan, J. C. Smith, L. Petridis, *Phys. Chem. Chem. Phys.* **2015**, *17*, 358–364.
[2] S. Sharma, A. Kumar, in *Lignin*, Springer International Publishing, Switzerland, **2020**, pp. 1–40.
[3] M. Niaounakis, E. Kontou, S. Pispas, M. Kafetzi, D. Giaouzi, *Polym. Eng. Sci.* **2019**, *59*, E432–E441.
[4] J.-W. Rhim, P. K. W. Ng, *Crit. Rev. Food Sci. Nutr.* **2007**, *47*, 411–433.
[5] N. Gontard, C. Duchez, J.-L. Cuq, S. Guilbert, *Int. J. Food Sci. Technol.* **1994**, *29*, 39–50.
[6] J. Han, *Edible films and coatings In Elsevier eBooks* **2014**. pp. 213–255.
[7] R. J. Avena-Bustillos, J. M. Krochta, *J. Food Sci.* **1993**, *58*, 904–907.
[8] H. Watanabe, A. Fujimoto, A. Takahara, *Polym. J.* **2014**, *46*, 216–219.
[9] F. Zhang, H. Y. Low, *Langmuir* **2007**, *23*, 7793–7798.
[10] Q. F. Xu, B. Mondal, A. M. Lyons, *ACS Appl. Mater. Interfaces* **2011**, *3*, 3508–3514.
[11] N. A. Patankar, *Langmuir* **2003**, *11* (4), 1249–1253.
[12] B. He, N. A. Patankar, J. Lee, *Langmuir* **2003**, *19*, 4999–5003.
[13] M. Miwa, A. Nakajima, A. Fujishima, K. Hashimoto, T. Watanabe, *Langmuir* **2000**, *16*, 5754–5760.
[14] P. G. de Gennes, *Rev. Mod. Phys.* **1985**, *57*, 827–863.
[15] T. Young, *Philos. Trans. R. Soc. London.* **1805**, *95*, 65–87.
[16] R. N. Wenzel, *Ind. Eng. Chem.* **1936**, *28*, 988–994.
[17] A. B. D. Cassie, S. Baxter, *Trans. Faraday Soc.* **1944**, *40*, 546.
[18] E. Bormashenko, R. Pogreb, T. Stein, G. Whyman, M. Erlich, A. Musin, V. Machavariani, D. Aurbach, *Phys. Chem. Chem. Phys.* **2008**, *10*, 4056–4061.
[19] R. E. Johnson, R. H. Dettre, in *Advances in Chemistry, Vol. 43*, American Chemical Society, Washington, D. C., **1964**, pp. 112–135.
[20] J. Eick, R. Good, A. Neumann, *J. Colloid Interface Sci.* **1975**, *53*, 235–248.
[21] J. Long, M. N. Hyder, R. Y. M. Huang, P. Chen, *Adv. Colloid Interface Sci.* **2005**, *118*, 173–190.
[22] E. L. Decker, S. Garoff, *Langmuir* **1997**, *13*, 6321–6332.
[23] R. H. Dettre, R. E. Johnson, *J. Phys. Chem.* **1965**, *69*, 1507–1515.
[24] M. Shanahan, C. Bourgès, *Int. J. Adhes. Adhes.* **1994**, *14*, 201–205.
[25] R. V. Sedev, J. G. Petrov, A. W. Neumann, *J. Colloid Interface Sci.* **1996**, *180*, 36–42.
[26] S. Su, M. Duhme, R. Kopitzky, *Materials* **2020**, *13*(21), 4897.
[27] J. Jian, Z. Xiangbin, H. Xianbo, *Adv. Ind. Eng. Polym. Res.* **2020**, *3*, 19–26.
[28] K. Elfehri Borchani, C. Carrot, M. Jaziri, *Composites Part A* **2015**, *78*, 371–379.
[29] Y.-F. Shih, R.-J. Jeng, *Polym. Int.* **2004**, *53*, 1892–1898.
[30] K. Weber, V. Wegmann, C. Mayer, M. Hilt, *Prog. Org. Coat.* **2018**, *122*, 154–158.
[31] R. Al-Itry, K. Lamnawar, A. Maazouz, *Polym. Degrad. Stab.* **2012**, *97*, 1898–1914.
[32] B. Bhushan, in *Encyclopedia of Nanotechnology*, Bd. 2nd ed., Springer Netherland, Berlin, **2016**, pp. 2831–2836.
[33] A. Marmur, *Langmuir* **2003**, *19*, 8343–8348.

Manuscript received: April 27, 2023
Revised manuscript received: July 18, 2023
Accepted manuscript online: July 19, 2023
Version of record online: ■■, ■■

RESEARCH ARTICLE

The surface topography of biopolymer foils is modified by mechanical imprinting on a submillimeter length scale. The created patterns strongly influence the wetting behavior and allow the preparation of hydrophobic surfaces with controlled solid-liquid interaction. The mechanical pressure can lead to a redistribution of individual constituents of the biopolymer blend in a surface-near region.

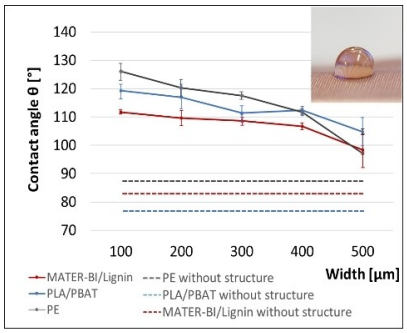

H. Liu, M. Zagler, Prof. Dr. M. Nase, Prof. Dr. K. Weber*, Prof. Dr. J. Albrecht**

1 – 10

Creating Hydrophobic Foils From Biopolymer Blends Using Mechanical Microimprinting